RSS Technical Report 111313 November 13, 2013

Improvements to the Vector Wind Climate Record Using RapidScat as a Common Reference and Aquarius/SMAP for High Winds in Rain

Frank J. Wentz
Remote Sensing Systems, Santa Rosa CA

Lucrezia Ricciardulli
Remote Sensing Systems, Santa Rosa CA

Remote Sensing Systems
444 Tenth Street, Suite 200, Santa Rosa, CA 95401 (707) 545-2904

Summary

This document describes on-going OVWST research and product generation at Remote Sensing Systems. Research is directed towards improving the vector wind (VW) retrievals coming from satellite microwave scatterometers. The research elements include (1) the geophysical model function (GMF) that relates radar backscatter to the VW, (2) the diurnal variability of VW particularly as it relates to the intercalibration of scatterometers, and (3) the effect of high winds and rain on VW retrievals. With respect to product generation, we describe our plans to add the VW datasets from ASCAT-B, OSCAT, and RapidScat to the existing collection of VW datasets for ERS-1, NSCAT, QuikScat, SeaWinds, and ASCAT-A.

With the ever increasing number of scatterometers in operation, we are putting more focus on bringing uniformity to the various VW datasets so that these datasets can be used as a combined multi-sensor product. To achieve this consistency, we will first establish a common wind speed reference for all scatterometers. This will be done by using wind speed retrievals from the large array of past, present, and future satellite microwave radiometers. These multi-decadal, multi-sensor wind retrievals are part of the NASA-sponsored Ocean Products Earth System Data Record (OP-ESDR). The OP-ESDR is a well-established climate product that is widely used by the Earth Science Community.

Once all VW datasets are intercalibrated to the OP-ESDR, we will do a more detailed analysis using NASA's new RapidScat as a common VW reference. For the first time, RapidScat will provide an abundance of near coincidence comparisons of VW retrievals from L-, C-, and Ku-band scatterometers. We expect the RapidScat comparisons will reveal small inconsistencies in the L-, C-, and Ku-GMFs that were not apparent from the OP-ESDR analysis. Based on these RapidScat results, we will fine-tune the GMFs and possibly elements of the retrieval algorithm.

The new L-band scatterometer/radiometer sensor complements on Aquarius and SMAP in conjunction with RapidScat will allow us to do a very detailed analysis of the VW retrievals in rain and high winds. The L-band wind speed retrievals are insensitive to rain and at the same time they are responsive to winds up to 50 m/s. The near coincident collocations between RapidScat and Aquarius/SMAP may provide the most comprehensive information on the effect of rain and high winds on Ku-band scatterometers to date. These results will be factored into improvements to the GMFs and possibly to the VW retrieval algorithm.

One concern is that our various calibration procedures and fine-tuning exercises will tend to diminish or alter the true diurnal variability of ocean winds. We will assess this potential problem by comparing the diurnal variations seen in the collection of scatterometers with the diurnal variability that will be provided by RapidScat. If inconsistencies are found, then this problem will need to be resolved.

Once the above research elements are completed and the necessary improvements are made to the GMFs and retrieval algorithm, all VW datasets will then be reprocessed to obtain improved and more consistent VW retrievals. These datasets will then be combined into an Ocean VW Climate Data Record (OVW-CDR). This will be done in coordination with the OWVST Climate Working Group.

We are also proposing a study to better understand the underlying physics of microwave scattering from a rough sea surface and to develop a single unified GMF that can be applied over the entire spectral band from 1.4 to 14 GHz. As an outcome of this investigation, we will have GMFs at 3 separate frequencies (L, C, and Ku) derived in a completely consistent manner (same analyses, same VW retrieval algorithm, same people), and hence the spectral differences in the GMFs should reflect the true spectral differences in the physics of radar backscatter.

Table of Contents

1 Objectives

This investigation is a continuation of our on-going OVWST research and data product generation. As in the past, the emphasis of the research is directed towards improving the vector wind (VW) retrievals coming from the existing array of satellite scatterometers. The research elements include (1) the geophysical model function (GMF) that relates radar backscatter to the VW, (2) the diurnal variability of VW particularly as it relates to the intercalibration of scatterometers, and (3) the effect of high winds and rain on VW retrievals. In addition, with the ever increasing number of scatterometers in operation, we are putting more focus on bringing uniformity to the various VW datasets so that these datasets can be used as a combined multi-sensor product, thereby substantially increasing the temporal sampling for scientific applications.

Table 1 lists the various scatterometers that are considered in this investigation. VW datasets for 6 scatterometers will be available at the end of our current OVWST funding cycle. As part of this proposed investigation, we will be adding ASCAT-B, OSCAT, and RapidScat.

To bring consistency to the VW datasets, we will first establish a common wind speed reference for all of the scatterometers listed in Table 1. This will be done by using wind speed retrievals from the large array of satellite microwave radiometers. These multi-decadal, multi-sensor wind retrievals are part of the NASA-sponsored Ocean Products Earth System Data Record (OP-ESDR). The OP-ESDR is a well-established climate product that is widely used by the Earth Science Community, and it provides a very useful wind speed reference for this scatterometer investigation.

Once all VW datasets are intercalibrated to the OP-ESDR, we will do a more detailed analysis using NASA's new RapidScat as a common VW reference. For the first time, RapidScat will provide an abundance of near coincidence comparisons of VW retrievals from L-, C-, and Ku-band scatterometers. We expect the RapidScat comparisons will reveal small inconsistencies in the L-, C-, and Ku-GMFs that were not apparent from the OP-ESDR analysis. Based on these RapidScat results, we will fine-tune the GMFs and possibly elements of the retrieval algorithm.

The new L-band scatterometer/radiometer sensor complements on Aquarius and SMAP in conjunction with RapidScat will allow us to do a very detailed analysis of the VW retrievals in rain and high winds. The L-band wind speed retrievals are insensitive to rain and at the same time they are responsive (i.e. do not saturate) to winds up to 50 m/s. The near coincident collocations between RapidScat and Aquarius/SMAP may provide the most comprehensive information on the effect of rain and high winds on Ku-band scatterometers to date. These results will be factored into improvements to the GMFs and possibly to the VW retrieval algorithm.

One concern we have is that our various calibration procedures and fine-tuning exercises will tend to diminish or alter the true diurnal variability of ocean winds. In other words, bringing consistency to VW retrievals of scatterometers observing the ocean at different times of day runs the risk of 'calibrating out' the natural diurnal differences. We will assess this potential problem by comparing the diurnal variations seen in the collection of scatterometers listed in Table 1 with the diurnal variability that will be provided by RapidScat. One of RapidScat's key objectives is to map out the diurnal cycle of winds over the oceans. If inconsistencies are found between the

diurnal variability inferred from RapidScat and that from the other scatterometers, then this problem will need to be resolved.

Once the above research elements are completed and the necessary improvements are made to the GMFs and retrieval algorithm, all VW datasets will then be reprocessed to obtain improved and more consistent VW retrievals. These datasets will then be combined into an Ocean VW Climate Data Record (OVW-CDR). This will be done in coordination with the OWVST Climate Working Group. The goal of this group is to advance our understanding of the many issues related to constructing an OVW-CDR, thereby leading to improved CDRs that better serve the needs of the climate research community.

We are also studying the spectral dependence of the backscattering from the ocean surface. As an outcome of this investigation, we will have GMFs at three separate frequency bands (L, C, and Ku). These 3 GMFs will be derived in a completely consistent manner (same analyses, same VW retrieval algorithm, and same group of people) and hence the spectral differences in the GMFs should reflect the true spectral differences in the physics of radar backscatter. Our goal is to better understand the underlying physics of microwave scattering from a rough sea surface and to develop a single unified GMF that can be applied over the entire spectral band between 1.4 and 14 GHz.

Table 1. Scatterometers Considered in this Investigation

Scatterometer	Frequency (GHz)	Launch	End of Operation	Ascending Node Time	Status of VW Dataset
ERS-1	5.3	Jul 1991	Apr 1996[1]	22:30	In Progress
ERS-2	5.3	Apr 1995	Jun 2003[2]	22:30	Not Proposed
NSCAT	14.0	Aug 1996	Jun 1997	22:30	In Progress
QuikSCAT	13.4	Jun 1999	Nov 2009[3]	6:00	Completed
SeaWinds	13.4	Dec 2002	Oct 2003	22:30	In Progress
ASCAT-A	5.3	Oct 2006	operating	21:30	Completed
OSCAT	13.5	Sep 2009	operating	24:00	Proposed
Aquarius	1.26	Jun 2011	operating	18:00	Completed
ASCAT-B	5.3	Sep 2012	operating	21:30	Proposed
RapidScat	13.4	TBD 2014	n/a	All times	Proposed
SMAP	1.2	TBD 2014	n/a	18:00	Separately Proposed

Notes to Table 1. A status of 'Completed' means VW dataset is currently available to the community. A status of 'In Progress' means the VW dataset will be available at the end of our current OVWST funding cycle, which is September 2014. SMAP work will be done as part of our 'Salinity from SMAP' Proposal. The Aquarius and SMAP datasets are just wind speed (no direction). (1) ERS-1 was switched off in June 1996 and retired in March 2000. (2) ERS-2 onboard tape recorder failed in June 2003, limiting the amount of data available. The instrument was taken out of service in September 2011. ERS-2 is not being proposed for reasons discussed in Section 1.2.8. (3) QuikSCAT still operates in a non-spinning mode.

2 Technical Approach and Methodology

2.1 Vector Wind versus Surface Wind Stress

Scatterometers measure surface roughness, and surface roughness is more closely correlated with surface stress τ than the actual wind speed at 10 m. For this reason, scatterometer wind retrievals are usually defined as the 10-m equivalent neutral wind, called $\mathbf{U}_{10EN}$, rather than the actual 10-m wind $\mathbf{U}_{10}$. To obtain $\mathbf{U}_{10}$ from $\mathbf{U}_{10EN}$ one needs information on the stability of the boundary layer, which is not contained in the scatterometer measurements.

The relationship between $\mathbf{U}_{10EN}$ and surface stress $\boldsymbol{\tau}$ depends on the air density ρ. For the same $\mathbf{U}_{10EN}$, cold heavy air will produce more stress (and roughness) than lighter warmer air. This effect is expressed by the surface stress equation:

$$\boldsymbol{\tau} = \rho C_{D10} \left|\mathbf{U}_{10EN}\right| \mathbf{U}_{10EN} \tag{1}$$

where C_{D10} is the neutral stability drag coefficient at a height of 10m and is a function of $\mathbf{U}_{10EN}$. Currently, most $\mathbf{U}_{10EN}$ retrieval algorithms, including ours, do not consider variations in ρ. Assuming that σ_o measurements are more a measure of $\boldsymbol{\tau}$ than $\mathbf{U}_{10EN}$, the ρ correction for $\mathbf{U}_{10EN}$ takes the form

$$\mathbf{U}_{10EN} = \sqrt{\frac{\langle\rho\rangle}{\rho}}\ \mathbf{U}_{10EN,retrieval} \tag{2}$$

where $\mathbf{U}_{10EN,retrieval}$ denotes the current set of VW retrievals, ρ is the air density for the given observation, and $\langle\rho\rangle$ is the average air density over the ensemble of scatterometer measurements used to derive the retrieval algorithm (≈1.2 kg/m^3). One convincing means to validate the hypothesis of density perturbation being already present in the scatterometer retrievals would be to use in situ wind stress measurements collocated with scatterometer data. Dr. Bourassa has provided us with an in situ $\boldsymbol{\tau}$ dataset derived from NDBC measurements, and OVWST investigators Edson and Vandemark are creating another in situ $\boldsymbol{\tau}$ dataset from long-term buoy flux measurements. Future collaboration with these investigators is envisaged to further address the topic. If equation (2) is substantiated, the correction will be applied to all VW datasets using NCEP surface temperature, humidity, and pressure fields to specify ρ for each VW retrieval.

Combining (1) and (2) gives

$$\boldsymbol{\tau} = C_{D10} \langle\rho\rangle \left|\mathbf{U}_{10EN,retrieval}\right| \mathbf{U}_{10EN,retrieval} \tag{3}$$

It is interesting to see that one can use the current $\mathbf{U}_{10EN,retrieval}$, as is, to compute stress without any need for information on air density (except for some single global value $\langle\rho\rangle$). This is to be expected because of the assumption that the σ_o measurements are more closely correlated with $\boldsymbol{\tau}$ than with $\mathbf{U}_{10EN}$ and hence information on air density is not needed.

Equation (3) provides the means to convert the $\mathbf{U}_{10EN}$ datasets into $\boldsymbol{\tau}$ datasets, assuming one has a reliable model for C_{D10}. So the VW datasets described herein serve the role of both a $\mathbf{U}_{10EN}$ dataset and a $\boldsymbol{\tau}$ dataset.

2.2 OP-ESDR as a Wind Speed Calibration Reference for Scatterometers

The calibration of the VW retrievals for the scatterometers listed in Table 1 is based to a large degree on the Ocean Products Earth System Data Record (OP-ESDR). The OP-ESDR is a suite of geophysical retrievals derived from satellite microwave radiometers. These retrievals include sea-surface temperature and wind speed, total water vapor and cloud water, and rain rate. The record starts in 1987 with the launch of the first SSM/I and continues to present with 7 radiometers currently operating (1 SSM/I, 3 SSM/IS, TMI, WindSat, AMSR-2) and another radiometer (GMI) to be launched in 2014. The L-band radiometers, Aquarius and SMAP, will be added in the near future. Figure 1 shows this collection of microwave radiometers. The 27-year OP-ESDR is freely available from www.remss.com and is widely used by the Earth Science Community. We acknowledge the many years of support that NASA's Earth Science Division has invested in the OP-ESDR.

Several of the radiometers shown in Figure 1 have proven to be very stable sensors, in part due to their local ascending node time not drifting. These sensors are: F08 and F13 SSM/I, F17 SSM/IS, WindSat, AMSR-E, and AMSR-2. They form the backbone to the time series. Two other radiometers, TMI and the soon-to-be-launched GMI, fly in inclined orbits and sample the entire 24-hour diurnal cycle. This diurnal sampling is helpful for the diurnal analysis described in Section 1.2.7. GMI will be particularly useful for calibrating the scatterometers. GMI will likely be the best calibrated satellite microwave radiometer to date due to its on-board dual calibration system. In addition, its spatial resolution is a factor of two better than its predecessor TMI. Due to the inclined orbit, the GMI swath will cross the ASCAT and OSCAT swath twice per orbit with a maximum observation time difference of ± 50 minutes.

The wind speed component of the OP-ESDR has been extensively evaluated by the research community. See Section 2.2 for a list of references related to the evaluation and usage of the OP-ESDR wind speed. The fundamental calibration of the OP-ESDR winds is moored ocean buoys. When averaged globally over the mission life, the satellite minus buoy wind speed difference is less than 0.1 m/s (a consequence of the calibration procedure) and the standard deviation is about 1 m/s, depending on the mix of buoys. When wind speeds from the different satellites shown in Figure 1 are compared, monthly averages show an inter-satellite difference on the order of 0.1 m/s. The 2-sigma error in deriving trends from the OP-ESDR is about 0.1 m/s/decade [*Wentz et al*., 2007].

The OP-ESDR also provides rain rate, which is used to exclude rainy areas from the VW calibration process. Rain affects C-band and Ku-band scatterometer observations [*Stiles and Yueh*, 2002; *Weissman*, 2002*; Hilburn and Wentz*, 2006; *Weissman and Bourassa*, 2008; *Portabella et al.*, 2012], and it also degrades the radiometer wind speed retrieval. So it is best to not use observations when rain is present.

The OP-ESDR provides us with a reference wind speed for the derivation of the scatterometer GMF. The GMF is derived so that the resulting scatterometer wind speed retrievals equal, on average, the OP-ESDR wind over the full range of wind speeds. To specify the OP-ESDR wind speed, we choose the radiometer wind speed retrievals that are closest in time to the scatterome-

ter measurement. Given the extensive array of microwave radiometers operating at different local times, good collocations are generally available (see next section). Deriving the GMF in this way brings consistency to the radiometer and scatterometer wind speed retrievals. The GMF derivation also requires wind direction, which is not part of the OP-ESDR. The handling of wind direction and the general methodology for the GMF derivation is described in the next section.

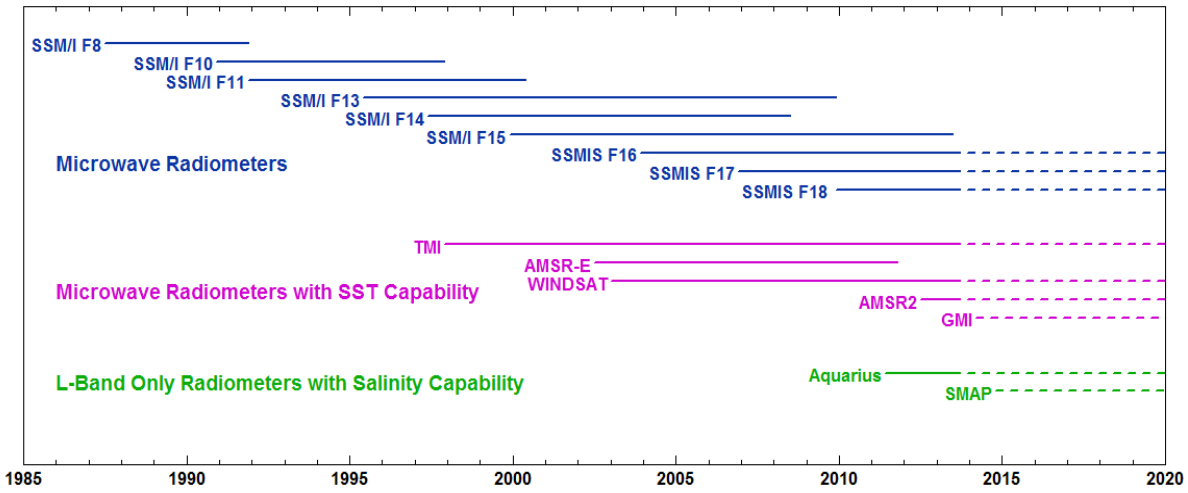

Fig 1. Satellite microwave radiometers used in the production of the OP-ESDR.

2.3 Derivation of L-, C-, and Ku-Band Geophysical Model Functions

The geophysical model function (GMF) is a key component of the vector wind (VW) retrieval algorithm. It relates radar backscatter cross section σ_o to wind speed w and the relative wind direction φ, which is defined as the wind direction minus the observing azimuth angle. It is also a function of the following sensor parameters: frequency, polarization and incidence angle. In general, the GMF is represented by a harmonic function of φ

$$\sigma_0 = \sum_{k=0}^{K} A_k(w)\cos(k\varphi) \tag{4}$$

where the A_k coefficients are explicit functions of the wind speed and implicit functions of frequency, polarization and incidence angle. Typically, the higher order terms for k>2 account only for 2-4% of the total variance, but for some cases their contribution can be as large as 10% (i.e., v-pol, crosswind, 10 m/s). Our GMF includes terms up to K=5. GMFs for scatterometers have been developed by a number of investigators over the years [*Wentz et al.*, 1984; *Freilich and Dunbar*, 1993; *Wentz and Smith*, 1999; *Yueh et al.*, 2001; *Draper and Long*, 2004; *Hersbach et al.*, 2007, *Isoguchi and Shimada*, 2009*; Hersbach*, 2010*; Yueh et al.*, 2010*; Ricciardulli and Wentz*, 2013a; *Meissner and Wentz*, 2013].

The derivation of the GMF requires that both wind speed and direction be specified. However, it is the wind speed specification that presents special problems for the GMF derivation.

Errors in specifying the reference wind speed can be systematic (i.e., a constant negative bias for high winds, a positive bias for the lower winds). To specify the GMF wind speed component, we use the wind speeds from the OP-ESDR described in the previous section. In contrast, errors in specifying wind direction by their nature tend to be random and have less effect on the calibration. Also errors in wind direction are less susceptible to long-term drifts.

Wind direction is not part of the OP-ESDR, so it must be obtained elsewhere. We use wind directions from two sources: NCEP 6-hour GDAS wind fields and the Cross-Calibrated, Multi-Platform (CCMP, [*Atlas et al*, 2011]) winds which incorporate ECMWF fields. The A_1 through A_5 coefficients specify the directional part of the GMF. The traditional way of determining these coefficients is to simply regress the observed σ_0 versus the relative wind direction φ for different wind speed bins thereby making a table of A_i versus wind. However, errors in the NCEP and ECMWF wind fields produce errors in φ and this leads to a systematic underestimation of the coefficients A_i. This is a well-known statistical artifact of harmonic regression. We compensate for this effect by fine-tuning the A_i coefficients using the histogram technique described in *Wentz and Smith* [1999] and *Ricciardulli and Wentz* [2013a].

As a final verification of the GMF's wind direction component, we analyze polar histograms of the wind direction retrievals relative to the satellite flight direction, which is a visualization method introduced by *Ebuchi* [1999, 2000] that is commonly referred to as Ebuchi plots. The difference of wind direction retrieval minus the flight direction is particularly sensitive to errors in specifying A_1 and A_2. In contrast, any errors in the NCEP or ECMWF wind direction will be uncorrelated with the flight direction of a particular scatterometer. Thus, a comparison of scatterometer versus NCEP Ebuchi plots is used to diagnose errors in the wind direction part of the GMF. Via trial and error, the $A_{1\text{-}2}$ coefficients are adjusted to match the NCEP Ebuchi plots.

In summary, the derivation of the GMF's wind direction component can be done using numerical models such as NCEP and ECMWF. However, the derivation of the GMF's wind speed component requires a precise calibration reference for wind speed. Our choice for this wind speed calibration reference is the OP-ESDR, which is tied to ocean buoy measurements. Ocean buoy measurements are not directly used for the GMF derivation because of their limited spatial distribution. However, the buoys are used to validate the various VW datasets, and in some sense they represent a withheld data set for final validation.

As part of our current OVWST and Aquarius funding, we have derived separate GMFs for L-, C-, and Ku-band. These 3 GMFs are based on the backscatter measurements from Aquarius, ASCAT-A, and QuikSCAT, respectively. All 3 GMFs are freely available from Remote Sensing Systems (RSS). Separate GMFs are needed for the three frequency bands because the scattering properties of the ocean surface depend on the radiation wavelength.

Aquarius, ASCAT-A, and QuikSCAT are called the 'reference scatterometers' because they were used to derive the GMFs. Since the GMFs were derived so as to match the scatterometer wind retrieval to OP-ESDR wind speed, the VW datasets for the reference scatterometers are intercalibrated to the OP-ESDR. However, when we apply these GMFs to other scatterometers,

intercalibration is not automatic because of relative biases between the σ_o measurements of different scatterometers operating in the same frequency band. For example, when we apply the C-band GMF derived from ASCAT-A to ERS-1, we need to account for relative biases in the ASCAT-A versus ERS-1 σ_o measurements. The intercalibration of the non-reference scatterometers is discussed in the next section.

Figure 2 shows the A_0 coefficient, at selected incidence angles, plotted versus wind speed for the L-, C-, and Ku-GMFs. We also show the A_0 coefficient from the European CMOD5.n GMF [*Hersbach, 2010*]. The major difference between our C-GMF and CMOD5.n is at the higher winds. The steeper A_0 curve of CMOD5.n is the reason why the CMOD5.n VW retrievals at high winds are appreciably lower than ours. It is our understanding that the Europeans plans to use a revised GMF with a less steep A_0 in their next reprocessing of ASCAT to correct the high wind problem. Figure 2 also shows that there is a large difference between the L- and C-GMFs. The L-GMF shows a much steeper A_0 curve at low to moderate winds than the C-GMF. We will relate these spectral differences in the GMFs to the underlying physics, as discussed in Section 1.2.9.

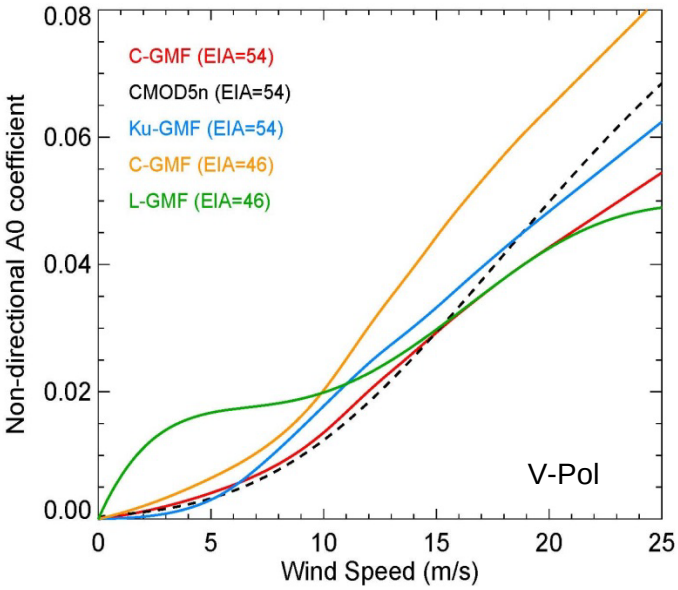

Fig. 2. A comparison of GMFs for different spectral bands.

Our Ku-GMF has a long history. It was first developed for NSCAT by *Wentz and Smith* [1999]. It was then improved by using QuikSCAT observations [*Ricciardulli and Wentz*, 2013a]. The 11 years of QuikSCAT data, as compared to one year of NSCAT data, allowed us to fine-tune the GMF. The new GMF is called Ku-2011. One major improvement of Ku-2011 was more realistic winds above 15 m/s. Another was that Ku-2011 is derived using the OP-ESDR winds as a reference. As a result the QuikSCAT wind speed retrievals are precisely calibrated to the OP-ESDR winds (see next section). For QuikSCAT, the OP-ESDR radiometers closest in time are WindSat, F13 SSM/I, and F17 SSM/IS. Ku-2011 was delivered to JPL and was used in their recent reprocessing of QuikSCAT [*Fore et al.*, 2013].

The Ku-2011 GMF is specified for the QuikSCAT incidence angles of 46.3° (H-pol) and 54.1° (V-pol). Under separate funding, Ku-2011 is being extended to a wider range of incidence angles so that it can be applied to RapidScat and OSCAT. We call this extended GMF the Ku-GMF.

The C-band GMF was derived from 4 years of ASCAT-A measurements [*Ricciardulli and Wentz*, 2012, 2013b]. The F16 SSM/IS, which is the OP-ESDR radiometer having the best collocation time with ASCAT-A, was used to specify wind speed. The L-band GMF [*Meissner and Wentz*, 2013] is based on the two years of scatterometer measurements taken by Aquarius aboard SAC-D. For the L-band GMF derivation, WindSat and F17 SSM/IS wind speeds were used.

The fact that all 3 GMFs were derived using the same method (and by the same people) has certain advantages. First, the band-to-band differences exhibited by the 3 GMFs are mostly likely due to the sea-surface scattering properties being different over the 1.4 to 14 GHz spectral range rather than differences in the methodology of the derivations. This will make the analysis of the multi-band GMF in Section 1.2.9 more meaningful. Likewise, the consistency in the GMFs will translate into more consistent L-, C-, and Ku-band VW datasets.

2.4 Status and Production of VW Datasets

The derivation of the L-, C-, and Ku-GMFs for the reference scatterometers Aquarius, ASCAT-A, and QuikSCAT is completed, and VW datasets for these 3 sensors are available, except that Aquarius only provides wind speed, not direction. Figure 3 shows that the new Ku- and C-GMFs are indeed producing wind speed retrievals consistent with the OP-ESDR. This figure shows the timeseries of two wind speed differences: QuikScat minus WindSat, and ASCAT-A minus WindSat. The inter-satellite differences are confined to the ±0.1 m/s range, which confirms that in a global sense the 3 sensors are well calibrated with respect to wind speed.

Figure 4 shows global maps of the mean and standard deviation of the ASCAT minus QuikSCAT wind speed for one year, 2008. There is some regional biasing at high latitudes where the winds are strong. This may indicate that the $A_0(w)$ coefficient in the GMFs need to be slightly adjusted, but further investigation is required to verify that this feature is not an artifact of diurnal variability or something else related to the spatial/temporal collocation of ASCAT with QuikSCAT. Fine-tuning of the GMFs and reprocessing of the VW datasets is discussed in subsequent sections.

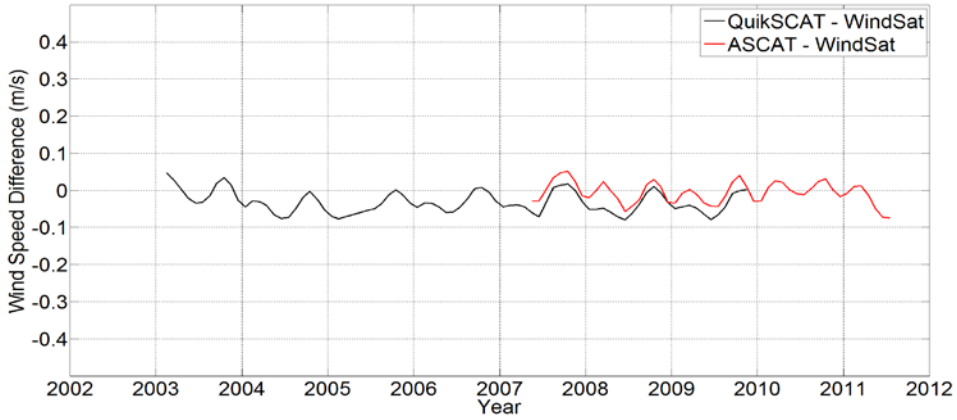

Fig 3. A comparison of QuikSCAT, ASCAT, and WindSat global mean wind speed.

We are now proceeding to apply the C-GMF derived from ASCAT-A to ERS-1. In doing this, we need to account for the fact that the fan-beam antenna pattern and other factors affecting the calibration of the σ_o measurements are different for ERS-1 as compared to ASCAT-A. Thus, we need to first adjust the ERS-1 σ_o measurements before applying the C-GMF. We anticipate that the adjustment will be a single multiplicative bias (i.e., a decibel offset) for each incidence angle cell along the fan-beam. We call this the σ_o fan-beam adjustment. The adjustment is done so that the ERS-1 wind speed retrieval agrees with the OP-ESDR wind over the full range of wind speeds. Once the σ_o fan-beam adjustment is completed, an ERS-1 VW dataset will be produced. This ERS-1 work will be completed by the end of our current funding cycle (Sep 2014).

We currently have VW datasets for NSCAT and SeaWinds, but they are now being reprocessed to incorporate the new Ku-GMF derived from QuikSCAT. These are short datasets (less than one year) but are still considered important. SeaWinds flew on ADEOS-2 in tandem with the microwave radiometer AMSR-A. This scatterometer/radiometer complement is unique and provides the opportunity to investigate the many synergisms associated with active-passive microwave remote sensing. As with the ERS-1 calibration, the Ku-GMF remains fixed and adjustments are made to the σ_o measurements to achieve consistency with the OP-ESDR wind speeds. This NSCAT/SeaWinds work will also be completed by the end of our current funding cycle.

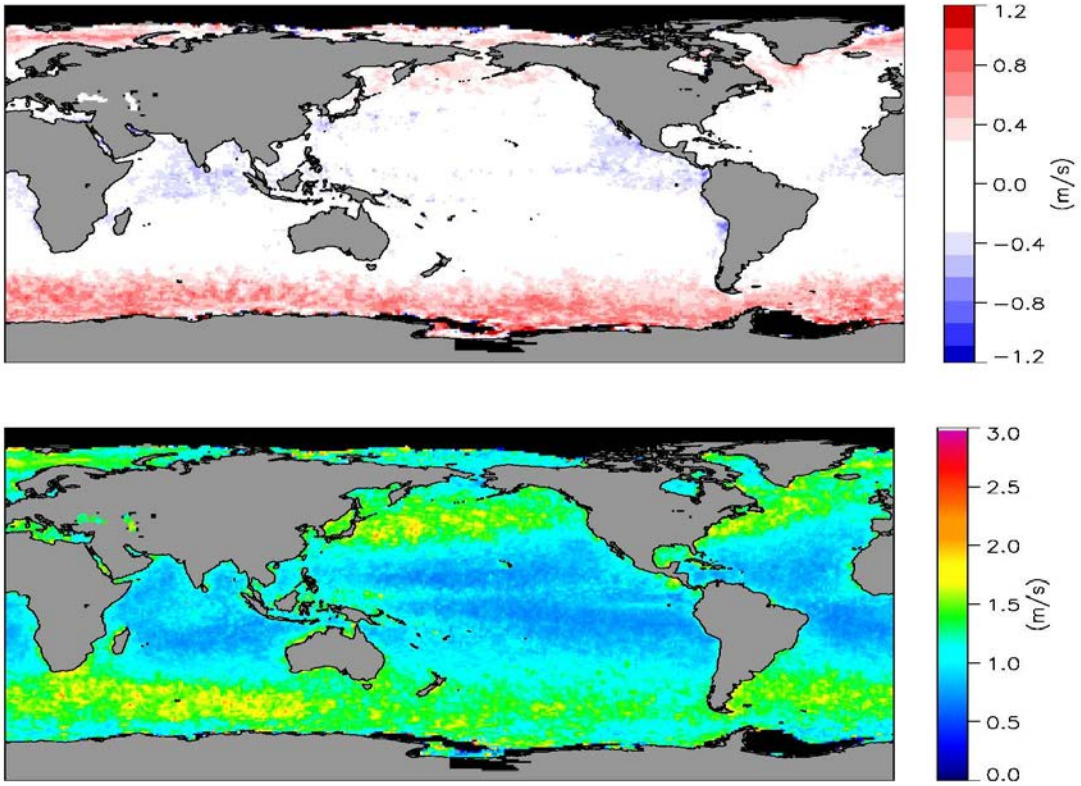

Fig. 4. Mean (top) and standard deviation (bottom) of the ASCAT - QuikSCAT wind speeds for 2008.

As part of our work we plan to produce intercalibrated VW datasets for ASCAT-B, OSCAT, and RapidScat. ASCAT-A and -B are nearly identical sensors and the C-GMF derived from ASCAT-A can be directly applied to ASCAT-B. A σ_o fan-beam adjustment to ASCAT-B may be needed, but we expect this to be small considering the sensor similarities. The QuikSCAT Ku-GMF, with the extension to a wider range of incidence angles, will be used for OSCAT. For OSCAT, we anticipate that a σ_o along-scan adjustment will be needed [*Long*, 2013]. This adjustment will again be based on the requirement that the OSCAT wind speed retrieval be consistent with the OP-ESDR winds. RapidScat will also use the Ku-GMF and we are hopeful that the only required σ_o adjustment will be two multiplicative biases, one to the inner beam and the other to the outer beam.

Current analyses being done by JPL [*Jaruwatanadilok*, 2013] and BYU [*Bradley and Long*, 2013] indicate that OSCAT has some unique calibration problems. These include the along-scan σ_o biases just mentioned above and steps in the σ_o timeseries due to changes in the processing algorithm [*Long*, 2013]. We are including Dr. Bryan Stiles at JPL as a collaborator to provide technical guidance related to OSCAT's calibration problems (see Section 1.2.12).

It should be emphasized that as each VW dataset is produced, an extensive validation is done with ocean buoys playing a major role. In this way, we ensure that the calibration procedure has not introduced any unexpected artifacts. Ocean buoy winds are primarily used for validation rather than calibration because they are point observations of limited spatial coverage, and limited measurements above 15 m/s.

The OP-ESDR calibration method is the first step in bringing consistency to the various scatterometer VW datasets. In subsequent sections, we described how further analyses, particularly those related to RapidScat, allow us to fine-tune the GMFs, σ_o adjustments, and possibly the retrieval algorithm to achieve even more consistency among the datasets.

2.5 Using RapidScat to Fine-Tune the GMFs and σ_o Adjustments

A major challenge to validating the proper intercalibration of the various VW datasets is that the sensors have different local observation times. For example, the local time of the ascending node for ASCAT is 9:30 pm, and for OSCAT it is midnight. Thus, there will typically be a 2.5 hour time difference for the OSCAT minus ASCAT collocations. This 2.5 hour difference can be significant. Systematic diurnal and semi-diurnal variations in wind can be misinterpreted as calibration error. Rain will also cause problems. Rain is highly variable in time and space and exhibits a strong diurnal cycle. In the 2.5 hours between an ASCAT observation and an OSCAT observation, rain features can significantly change.

NASA's new RapidScat provides the ideal means to circumvent the problems associated with the time differences. RapidScat will fly in a quasi-equatorial orbit between 50S and 50N, and its swath will cross the swaths of the other scatterometers twice each orbit. The maximum time difference at the crossover points will be ±50 minutes.

Once the various scatterometers are intercalibrated using the OP-ESDR methodology presented in Section 1.2.4, we will conduct a more detailed analysis of inter-scatterometer VW differences using RapidScat as a common reference. Since RapidScat will provide near coincident collocations with the other scatterometers, diurnal variability and changing rain patterns will no longer be issues, and we can look in greater detail at any residual inter-scatterometer differences in the VW fields. We expect this analysis may reveal small inconsistencies in the L-, C-and Ku-GMFs and in the σ_o adjustments that were not apparent from the OP-ESDR analysis.

To achieve consistency between the RapidScat and ASCAT-A/B VW fields, a 2-way perturbation analysis will be done to fine-tune the GMFs and the σ_o adjustments. For each collocation, the RapidScat VW will be converted to a synthetic σ_o using the C-GMF. Likewise, the ASCAT-A/B VW will be converted to a synthetic σ_o using the Ku-GMF. Then $\Delta\sigma_{o,C}$ and $\Delta\sigma_{o,Ku}$ denote the synthetic minus measured σ_o differences which will be correlated with wind speed w, the relative wind direction φ, and incidence angle. The C- and Ku-GMFs and the ASCAT-B σ_o fan-beam adjustments will be perturbed so as to simultaneously minimize $\Delta\sigma_{o,C}$ and $\Delta\sigma_{o,Ku}$. This '2-way' method is designed to treat RapidScat and ASCAT-A/B equally without assuming one is right and the other wrong. The result should be an improvement to both.

This procedure will be modified for the OSCAT/RapidScat collocations. Since OSCAT has unique calibration problems (see previous section), the perturbation analysis will be one-way: RapidScat will be a fixed reference and OSCAT will be adjusted to match RapidScat.

In addition to the near-coincident collocation provided by RapidScat, the orbits for ASCAT-A and ASCAT-B will also provide near simultaneous observations for one another. The MetOp-A and B spacecrafts operate in a co-planar orbit (i.e. same ascending node time), 174^o out of phase, and the ASCAT-A and -B swaths partially overlap with a 50 minute delay. Thus the VW fields from the two scatterometers can be overlaid and compared in the same way as described for RapidScat. We expect this ASCAT-A versus ASCAT-B analysis will provide an even better definition of the C-GMF and the σ_o fan-beam adjustment for ASCAT-B.

RapidScat will also cross over the swaths of the L-band scatterometers Aquarius and SMAP. The L-band scatterometer datasets only provide wind speed, so the crossover analysis is somewhat simpler. The major benefit of the L-band crossover analysis is that we can achieve the proper calibration of high winds (> 20 m/s) and better understanding of the effects of rain, both of which are discussed in the next section.

2.6 Using Tri-Band Scatterometry for Understanding Effects of Rain and High Winds

The extensive array of scatterometers operating in three spectral bands (L, C and Ku) provides the means to investigate two important aspects of scatterometry: (1) the effect of rain on scatterometer observations and (2) the retrieval of high winds. Since high winds and rain are often associated with each other, it is advantageous to consider both effects in unison.

The Aquarius and SMAP L-band scatterometers and radiometers are insensitive to the direct effect of rain (i.e., attenuation and scattering by rain drops) and have a relatively clear view of

the ocean surface through rain. At very high winds (above 25 m/s), the radiometer measurements have the advantage of not saturating, which was shown in the classic paper by W. Jones and C. Swift [*Jones et al.,* 1981]. The lack of saturation is due to the ocean brightness temperature (T_B) increasing approximately linearly with wind speed up to winds of 50 m/s. Thus, these L-band sensors play an important role in separating the effects of rain and high winds.

Although the direct effect of rain at L-band is very small, there is the possibility that rain hitting the ocean surface will create a 'splash effect' that will alter the ocean σ_o and T_B at L-band. However, the SMOS results reported by *Boutin et al.* [2013] indicate that the 'splash effect' at L-band is small compared to the higher frequencies because the 21-cm wavelength is much larger than the splash roughness scales. As part of our Aquarius investigation, we are also looking at the L-band splash effect, and it does appear to be small as evidenced by relatively accurate salinity retrievals when rain is present.

Figure 5 provides an example of Aquarius L-band high wind speed retrievals for three storms. There are two types of Aquarius retrievals: one that just uses the scatterometer measurements and another that uses both scatterometer and radiometer measurements (i.e., the active/passive retrieval) [*Meissner and Wentz*, 2013]. For two of the storms, we also show the WindSat all-weather retrievals which give good high-wind retrievals through rain [*Meissner and Wentz*, 2009]. Figure 5 shows that the scatterometer-only retrievals seem to lose sensitivity above 25 m/s while the active-passive L-band wind retrievals track WindSat and NOAA's Hurricane Research Division (HRD) winds quite well. The good agreement for these results also suggests that the splash effect is small at L-band.

Assuming the L-band splash effect is small, L-band active-passive measurements from Aquarius and SMAP will provide a reliable means to obtain winds in storms free of rain contamination. SMAP may prove to be particularly useful in this regard because the SMAP spatial resolution of 10-40 km (scatterometer, radiometer) and a large swath width (1000 km) are major improvements over Aquarius (100 km resolution and 390 km swath width).

We will use the active-passive L-band winds as a calibration reference for assessing the impact of rain on the Ku-band and C-band wind retrievals. For Ku-band, RapidScat provides an ideal platform for studying the impact of rain. A RapidScat swath will cross the Aquarius and SMAP swaths once every orbit, thereby providing ±50 minute (maximum) collocations on a regular basis. On such short time scales, the nature of the storm and high winds fields should be fairly constant. The collocated Ku-band versus L-band wind speed differences will be correlated with rain rate to assess the impact of rain at Ku-band. For Aquarius collocations, coincident rain rate information will be obtained from Aquarius' companion sensor: the 23/37 GHz microwave radiometer (MWR). For SMAP collocations, we will need to rely on WindSat and F17 SSM/IS to obtain near coincident rain rate. Both of these sensors have the same ascending node time as SMAP and Aquarius and hence should provide timely collocations.

We will also collocate ASCAT-A and ASCAT-B with SMAP and Aquarius to assess the effect of rain on C-band VW retrievals. However, in this case the time difference between the L-

band and C-band observations will be about 3.5 hours (see Table 1), which will make this analysis more difficult than for RapidScat, as rain can vary significantly in that time frame.

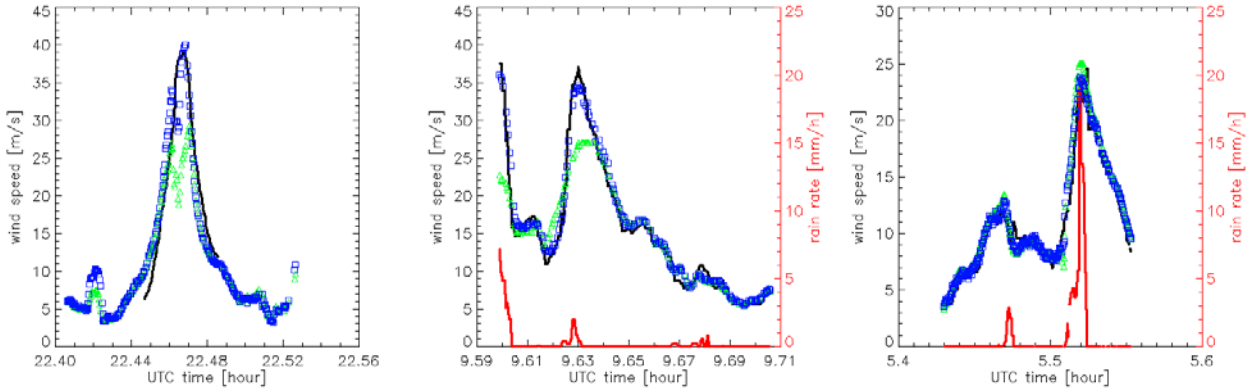

Fig. 5. Aquarius L-band wind speed retrievals for 3 storms: Hurricane Katia on 9/26/2011 (left) and 2 extra-tropical storms (middle and right). Blue squares are the Aquarius radiometer plus scatterometer retrievals and the green triangles are the scatterometer-only retrievals. The black lines represent either Hurricane Research Division (HRD) model winds (left) or WindSat 'all weather' winds (middle and right). The HRD model winds are shifted along the storm track to the time of the Aquarius overpass and resampled to the Aquarius resolution. The red lines are the WindSat rain retrievals.

2.7 Verifying that Scatterometer VW Datasets Display the Expected Diurnal Variability

One concern we have is that our various calibration procedures and fine-tuning exercises will diminish or alter the true diurnal variability of ocean winds. In other words, bringing consistency to VW retrievals of scatterometers observing the ocean at different times of day runs the risk of 'calibrating out' the natural diurnal differences. As a preliminary analysis of this potential problem, we used the combination of QuikScat and ASCAT-A VW datasets to infer the diurnal cycle. We first describe the methodology used for this analysis.

Let $f(h)$ express the diurnal variability of wind speed or its meridional or zonal component, where h is the local time of day (hours). The variability $f(h)$ is expressed as a Fourier series:

$$f(h) = D_0 + \sum_{n=1}^{N} D_n \cos\left[\frac{2\pi n(h - h_{on})}{24}\right] \tag{5}$$

where D_n and h_{on} are the amplitudes and phases. We call the first harmonic (n=1) the diurnal cycle and the second harmonic the semidiurnal cycle. Between 45S and 45N, the difference in the local observation time between the ascending and descending orbit segments is about 12 hours. Thus, the ascending minus descending difference for $f(t)$ is approximately

$$\Delta f(h) \equiv f(h) - f(h+12) = 2\sum_{n=odd}^{N} D_n \left\{\cos\left[\frac{2\pi n(h - h_{on})}{24}\right]\right\} \approx 2D_1 \cos\frac{2\pi(h - h_{o1})}{24} \tag{6}$$

By taking the ascending minus descending difference, all odd harmonics including the semidiurnal cycle cancel out. Furthermore, assuming the higher order even harmonics are small, one can use $\Delta f(h)$ as a good estimate for the diurnal cycle in the 45S to 45N zone. Since QuikSCAT and

ASCAT-A have different ascending node times (h=6:00 and h=21:30 respectively), one has two equations (6) for $\Delta f\,(h)$, from which the two unknowns D_1 and h_{o1} can be easily found.

Figure 6 compares the amplitude D_1 and phase h_{o1} of the wind speed diurnal cycle as inferred from the QuikSCAT/ASCAT-A with that from NASA's Reanalysis Project MERRA. The MERRA results are for 1990-1994 (what we had on hand), whereas the QuikSCAT/ASCAT-A results are for 2005-2011. In spite of the different time periods, there are a number of similarities between QuikSCAT/ASCAT-A and MERRA. Both show a significant diurnal amplitude in areas surrounding South Africa and South America, with average peak amplitude D_1 exceeding 0.5 m/s in some places. In these areas, the diurnal variations extend over a thousand kilometers away from the coast with the phase propagating later in the day as the distance from the coast increases, which is consistent with the idea of a propagating internal gravity wave [*Lerczak et al.*, 2001; *Gille et al.*, 2003, 2005; *Wood et al.*, 2009]. Similarities are also seen in other coastal regions along Australia, India and Central America where the average wind speed is low, and therefore more impacted by land-sea breeze diurnal variations.

Figure 6 also shows the amplitude and phase for the meridional component of wind speed as derived from QuikSCAT/ASCAT-A. The diurnal variation of the meridional component is out of phase in the two hemispheres (maxima at 7 am and 7 pm), and the amplitude is about 0.3 to 0.4 m/s. These results are quite consistent with those reported by the *Ueyama and Deser* [2008] analysis of the TAO buoy data, which suggest the diurnal variation in the meridional component originates from variations of the surface pressure field probably linked to the variability of tropical convection and the resulting reorganization of wind divergence/convergence patterns.

This preliminary look at the diurnal information in the QuikSCAT and ASCAT-A wind fields suggest that the calibration procedures we are using to derive the GMFs are preserving the diurnal cycle at least to some extent. These results say nothing about the semidiurnal cycle.

As part of our investigation, we will take a closer look at the diurnal variability in the various VW datasets derived from the polar-orbiting scatterometers. The analysis will be similar to that shown above for QuikSCAT and ASCAT. For example, the diurnal cycle will be determined from OSCAT and ASCAT, which have local observation times at 12:00 and 21:30. The OSCAT/ASCAT diurnal cycle will then be compared to QuikSCAT/ASCAT and to RapidScat, which is ideally suited for this type of diurnal analysis.

RapidScat will also allow us to assess the impact of the semi-diurnal cycle. The polar-orbiting scatterometers are affected by the semi-diurnal cycle, but unlike the diurnal cycle, it is not possible to uniquely infer the semi-diurnal cycle just given observations at four times during the day. The only reliable means to infer the semi-diurnal cycle is RapidScat. We will determine if any residual differences between QuikSCAT, ASCAT, and OSCAT can be explained by the semi-diurnal cycle inferred from RapidScat.

The primary objective of the diurnal analysis is to assess the consistency of the diurnal variability exhibited by the polar-orbiting scatterometers with that directly measured by RapidScat. Any obvious inconsistencies will need to be resolved.

The diurnal analysis will be supplemented by looking at the diurnal variability in wind speed obtained from the radiometers TMI and GMI. Similar to RapidScat, these two radiometers sample the 24-hour diurnal cycle every 40 days. The inclusion of TMI and GMI will provide a robust number of satellite observations for studying diurnal winds.

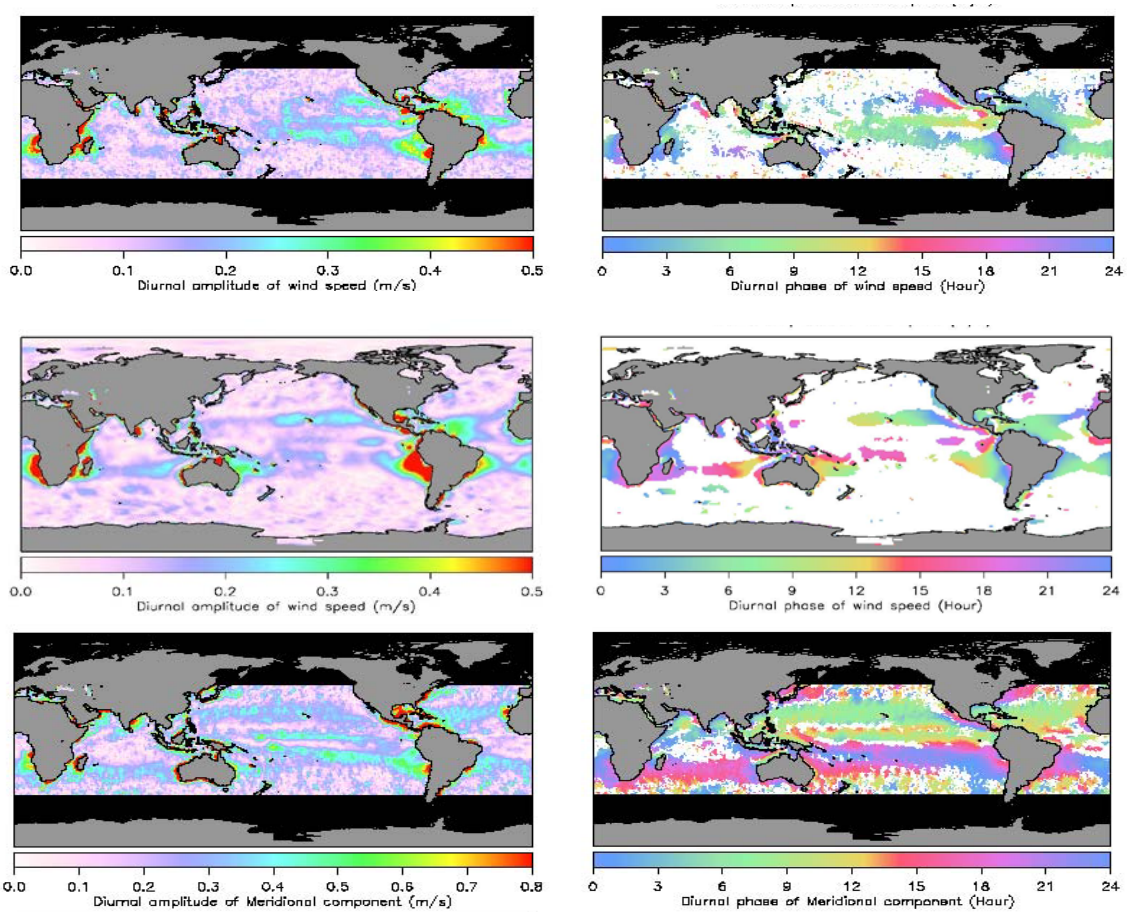

Fig. 6. Diurnal cycle of ocean winds derived from QuikSCAT/ASCAT-A and from MERRA. The left (right) column shows the amplitude (phase) of the diurnal cycle. The top (middle) row shows the QuikSCAT/ASCAT-A (MERRA) results for wind speed. The bottom row shows QuikSCAT/ASCAT-A results for the meridional component of wind.

2.8 Production and Distribution of the Ocean Vector Wind Climate Data Record

Once the above analyses are completed and we have final versions of the L-, C-, and Ku-GMFs along with final σ_o adjustments, we will reprocess the OV datasets for the scatterometers listed in Table 1. Our intention is to combine the various OV datasets into an Ocean Vector Wind Climate Data Record (OVW-CDR).

The production of the OVW-CDR will be done in coordination with the newly formed OWVST Climate Working Group. We will look to this group for advice, recommendations, and guidelines for constructing and validating the OVW-CDR. Of particular importance is determining what measures can be taken to enhance the construction of decadal records of the divergence

and curl of the wind stress field. For completeness, we would like to see the ERS-2 VW dataset be part of the OVW-CDR. We have not included it at this time because we have not yet worked with ERS-2 and it appears that ERS-2 has some special calibration/operational problems that we do not fully understand. We will seek advice from the Climate Working Group on how to proceed with ERS-2.

The production of the OVW-CDR will be completed towards the end of this investigation, and many details are still to be determined via the Climate Working Group. Our current vision is a daily gridded dataset at 1/4^o resolution common to all scatterometers subsetted according to ascending and descending orbit segments. All VW retrievals from the different scatterometers would be included, but not merged together. For example, if VW retrievals from two scatterometers are available at a given grid point, both retrievals would be included with appropriate indexing to identify the contributing scatterometer. The chi-squared values (i.e. SOS or MLE) for the retrievals will be included to facilitated quality control and rain flagging [*Portabella et al.*, 2012]. Coincident radiometer rain retrievals from the OP-ESDR will also be provided. For each retrieval, the observation time will be given and there will be no attempt to normalize the retrievals to a common time of day. Any higher level procedure for merging the VW would need to account for natural diurnal variability. The OVW-CDR product will be released in netCDF format with CF-compliant metadata so it is useful to the climate community.

2.9 Unified, Multi-Band Geophysical Model Function

The PI of this investigation began his career by developing a two-scale scattering model for the ocean surface [*Wentz*, 1975, 1977]. We are now at the point where we can revisit the basic underlying physics responsible for microwave backscattering. We have GMFs at three different frequency bands (1.3, 5.3, 13.4 GHz). All 3 GMFs were derived using the same assumptions and methods (and by the same people). Therefore, we expect the frequency dependence exhibited by the 3 GMFs to be a true indicator of the spectral characteristics of the physics rather than being due to different GMF derivation methodologies.

For an incidence angle of 45^o, simple Bragg scattering theory says the ocean wavelengths λ_{sea} responsible for backscattering are $\lambda_{sea} = \lambda/\sqrt{2}$, where λ is the radiation wavelength. Thus to a first order, the backscattering we are seeing at the 3 frequency bands is due to ocean waves having wavelengths of 17, 4, and 1.6 cm. The GMF A_0 coefficients shown in Figure 2 indicate that the growth of the longer ocean waves with wind is significantly different than that for the shorter ocean waves. For example, Figure 2 suggests that the 17-cm waves grow quickly up to about 4 m/s. The wind-speed response then flattens out between 4 and 10 m/s, and picks up again for higher winds. This is a much different wind speed response than shown by the shorter ocean waves. In addition, an analysis of the GMF A_1 and A_2 coefficients indicates that for L band cross-wind observations, there is no sensitivity of σ_o to wind speed for moderate winds. This is again quite different than at C- and Ku-band.

We will relate the spectral differences seen in the 3 GMFs to wind forcing of the sea-surface height wavenumber spectrum [*Elfouhaily et al.*, 1997; *Hwang et al.*, 2000]. This will be done in

the context of two-scale scattering theory [*Durden and Vesecky*, 1985, 1989]. We will also consider the L-, C- and Ku-band GMF for brightness temperature T_B [*Meissner and Wentz*, 2012, 2013]. The physics governing T_B is similar to that for σ_o except that it is the sea-surface slope wavenumber spectrum (rather than height spectrum) that plays the dominate role. Also at high winds, sea foam significantly affects the sea surface emission. Looking at both the σ_o and T_B GMFs over the frequency range from 1.3 to 14 GHz should give us a more complete understanding of the physical mechanisms that drive the backscatter and emission from a rough sea surface.

Using the knowledge gained for this analysis, we will combine the 3 GMFs into one model that provides σ_o over the entire range from 1.3 to 14 GHz. A similar analysis for the T_B GMF over the spectral range from 1.4 to 90 GHz is currently being done under separate funding.

3 References

Atlas, R. M., R. N. Hoffman, J. Ardizzone, S. M. Leidner, J. C. Jusem, D. K. Smith and D. Gombos, (2011) A Cross-Calibrated, Multi-Platform Ocean Surface Wind Velocity Product for Meteorological and Oceanographic Applications, *Bulletin of the American Meteorological Society, 92*(11), 157-174.

Boutin, J., N. Martin, G. Reverdin, X. Yin and F. Gaillard, (2013) Sea surface freshening inferred from SMOS and ARGO salinity: Impact of rain, *Ocean Science, 9*, 183-192, doi:10.5194/os-9-183-2013.

Bradley, J. P. and D. G. Long, (2013), Estimation of the OSCAT spatial response function using island targets. *IEEE Transactions on Geoscience and Remote Sensing,* in press.

Draper, D. W. and D. G. Long, (2004) Simultaneous Wind and Rain Retrieval Using SeaWinds Data, *IEEE Transactions on Geoscience and Remote Sensing, 42*, 1411-1423.

Durden, S. L. and J. F. Vesecky, (1985) A Physical Radar Cross-Section Model for a Wind-Driven Sea With Swell, *IEEE Journal of Oceanic Engineering, OE-10*(4), 445-451.

Durden, S. L. and J. F. Vesecky, (1989) On the Ability of Rough Surface Scattering Approximations to Predict Hydrodynamic Modulation of the Ocean Radar Cross Section: A Numerical Study, *J. Geophys. Res., 94*(C9), 12703-12708.

Ebuchi, N., (1999) Statistical Distribution of Wind Speeds and Directions Globally Observed by NSCAT, *Journal of Geophysical Research, 104*(C5), 11393-11403.

Ebuchi, N., (2000) Evaluation of NSCAT-2 Wind Vectors by Using Statistical Distributions of Wind Speeds and Directions, *Journal of Oceanography, 56*, 161-172.

Elfouhaily, T., B. Chapron, K. B. Katsaros and D. Vandemark, (1997) A Unified Directional Spectrum for Long and Short Wind-Driven Waves, *Journal of Geophysical Research, 102*(C7), 15781-15796.

Fore, A. G., B. W. Stiles, A. H. Chau, B. A. Williams, R. S. Dunbar and E. Rodriguez, (2013), Point-Wise Wind Retrieval and Ambiguity Removal Improvements for the QuikSCAT Climatological Data Set, *IEEE Transactions on Geoscience and Remote Sensing,* in press.

Freilich, M.H., and R. S. Dunbar, 1993: A preliminary C-band scatterometer model function for the ERS-1 AMI instrument. Proceedings of the First ERS-1 Symposium, Cannes, France, ESA, SP-359, 79–83.

Gille, S. T., (2005) Statistical Characterization of Zonal and Meridional Ocean Wind Stress, *Journal of Atmospheric and Oceanic Technology, 22*, 1353-1372.

Gille, S. T., S. G. L. Smith and S. M. Lee, (2003) Measuring the Sea Breeze From QuikSCAT Scatterometry, *Geophysical Research Letters, 30*(3), 1114, doi:10.1029/2002GL016230.

Hersbach, H., (2010) Comparison of C-Band Scatterometer CMOD5.N Equivalent Neutral Winds With ECMWF, *Journal of Atmospheric and Oceanic Technology, 27*, 721-736.

Hersbach, H., A. Stoffelen and S. de Haan, (2007) An Improved C-Band Scatterometer Ocean Geophysical Model Function: CMOD5, *Journal of Geophysical Research, 112*, C03006, doi:10.1029/2006JC003743.

Hilburn, K. A., F. J. Wentz, et al., (2006) Correcting active scatterometer data for the effects of rain using passive microwave data, *Journal of Applied Meteorology and Climatology, 45*, 382-398.

Hwang, P. A., D. W. Wang, E. J. Walsh, W. B. Krabill and R. N. Swift, (2000) Airborne Measurements of the Wavenumber Spectra of Ocean Surface Waves. Part I: Spectral Slope and Dimensionless Spectral Coefficient, *Journal of Physical Oceanography, 30*, 2753-2767.

Isoguchi, O., and M. Shimada (2009), An L-band ocean geophysical model function derived from PALSAR, *IEEE Transactions on Geoscience and Remote Sensing*, *47*(7), 1925-1936, doi:10.1109/TGRS.2008.2010864.

Jaruwatanadilok, S., B. W. Stiles and A. G. Fore, (2013) Cross calibration between QuikSCAT and Oceansat, *IEEE Transactions on Geoscience and Remote Sensing*, submitted.

Jones, W. L., P. G. Black, et al., (1981) Airborne microwave remote sensing measurements of hurricane Allen, *Science*, *214*, 274-280.

Lerczak, J. A., M. C. Hendershott and C. D. Winant, (2001) Observations and Modeling of Coastal Internal Waves Driven by a Diurnal Sea Breeze, *Journal of Geophysical Research, 106*(C9), 19715-19729.

Long, D., (2013). Personal Communication.

Meissner, T., and F. J. Wentz, (2009) Wind vector retrievals under rain with passive satellite microwave radiometers, *IEEE Transactions on Geoscience and Remote Sensing*, *47*(9), 3065-3083.

Meissner, T. and F.J. Wentz, (2012) The Emissivity of the Ocean Surface Between 6 - 90 GHz Over a Large Range of Wind Speeds and Earth Incidence Angles, *IEEE Transactions on Geoscience and Remote Sensing*, *50*(8), 3004-3026.

Meissner T., and F.J. Wentz, (2013) A geophysical model for the emission and scattering of L-band microwave radiation from rough ocean surfaces, *JGR Oceans Special Issue*, submitted.

Portabella, M., A. Stoffelen, Wenming Lin , A. Turiel, A. Verhoef, J. Verspeek and J. Ballabrera-Poy, (2012) Rain Effects on ASCAT-Retrieved Winds: Toward an Improved Quality Control, *IEEE Transactions on Geoscience and Remote Sensing*, *50*(7), 2495-2506.

Portabella, M., A. Stoffelen, A. Verhoef and J. Verspeek, (2012) A New Method for Improving Scatterometer Wind Quality Control, *IEEE Geoscience and Remote Sensing Letters*, *9*(4), 579-583.

Ricciardulli, L. and F. J. Wentz, (2012) Development of Consistent Geophysical Model Functions for Different Scatterometer Missions: Ku and C-band, paper presented at 2012 IOVWST meeting, Utrecht, Netherlands.

Ricciardulli, L. and F. J. Wentz, (2013a), A Scatterometer Geophysical Model Function for High Winds: QuikSCAT Ku-2011, *Journal of Atmospheric and Oceanic Technology*, submitted.

Ricciardulli, L. and F. J. Wentz, (2013b) Towards a Climate Data Record of Ocean Vector Winds: The New RSS ASCAT, paper presented at 2013 IOVWST Meeting, Kona, Hawaii.

Stiles, B. W. and S. H. Yueh, (2002) Impact of Rain on Spaceborne Ku-Band Wind Scatterometer Data, *IEEE Transactions on Geoscience and Remote Sensing*, *40*(9), 1973-1983.

Ueyama, R. and C. Deser, (2008) A Climatology of Diurnal and Semidiurnal Surface Wind Variations Over the Tropical Pacific Ocean Based on the Tropical Atmosphere Ocean Moored Buoy Array, *Journal of Climate, 21,* 593-607.

Weissman, D. E., (2002) Effects of Rain Rate and Wind Magnitude on SeaWinds Scatterometer Wind Speed Errors, *Journal of Atmospheric and Oceanic Technology*, *19,* 738-746.

Weissman, D. E. and M. A. Bourassa, (2008) Measurements of the Effect of Rain-Induced Sea Surface Roughness on the QuikSCAT Scatterometer Radar Cross Section, *IEEE Transactions on Geoscience and Remote Sensing, 46,* 2882-2894.

Wentz, F. J., (1975) A Two-Scale Scattering Model for Foam-Free Sea Microwave Brightness Temperatures, *Journal of Geophysical Research, 80*(24), 3441-3446.

Wentz, F. J. (1977), A Two-Scale Scattering Model With Application to JONSWAP '75 Aircraft Microwave Scatterometer Experiment, *NASA Contractor Report 2919*, 122pp., National Technical Information Service.

Wentz, F. J., S. Peteherych and L. A. Thomas, (1984) A Model Function for Ocean Radar Cross-Sections at 14.6 GHz, *IEEE Transactions on Geoscience and Remote Sensing, 89*(C3), 3689-3704.

Wentz, F.J., L. Ricciardulli, K.A. Hilburn and C.A. Mears, (2007) How Much More Rain Will Global Warming Bring?, *Science, 317,* 233-235.

Wentz, F. J. and D. K. Smith, (1999) A Model Function for the Ocean-Normalized Radar Cross Section at 14 GHz Derived From NSCAT Observations, *IEEE Transactions on Geoscience and Remote Sensing*, *104*(C5), 11499-11514.

Wood, R., M. Köhler, R. Bennartz and C. O'Dell, (2009) The Diurnal Cycle of Surface Divergence Over the Global Oceans, *Quarterly Journal of the Royal Meteorological Society, 135,* 1484-1493.

Yueh, S. H., S. J. Dinardo, A. G. Fore and F. K. Li, (2010) Passive and Active L-Band Microwave Observations and Modeling of Ocean Surface Winds, *IEEE Transactions on Geoscience and Remote Sensing, 48*(8), 3087-3100.

Yueh, S. H., B. W. Stiles, et al., (2001) QuikSCAT Geophysical Model Function for Tropical Cyclones and Applications to Hurricane Floyd, *IEEE Transactions on Geoscience and Remote Sensing, 39,* 2601-2612.